

Measurements of Atmospheric Antiprotons

K. Yamato ^a, K. Abe ^{a,1}, H. Fuke ^b, S. Haino ^c, Y. Makida ^c,
 S. Matsuda ^d, H. Matsumoto ^d, J.W. Mitchell ^e, A.A. Moiseev ^e,
 J. Nishimura ^d, M. Nozaki ^a, S. Orito ^{d,2}, J.F. Ormes ^e,
T. Sanuki ^{d,*}, M. Sasaki ^e, E.S. Seo ^f, Y. Shikaze ^{a,3},
 R.E. Streitmatter ^e, J. Suzuki ^c, K. Tanaka ^c, T. Yamagami ^b,
 A. Yamamoto ^c, T. Yoshida ^c, K. Yoshimura ^c

^a*Kobe University, Kobe, Hyogo 657-8501, Japan*

^b*The Institute of Space and Astronautical Science (ISAS) of Japan Aerospace
 Exploration Agency (JAXA), Sagamihara, Kanagawa, 229-8510, Japan*

^c*High Energy Accelerator Research Organization (KEK), Tsukuba, Ibaraki
 305-0801, Japan*

^d*The University of Tokyo, Bunkyo, Tokyo 113-0033, Japan*

^e*National Aeronautics and Space Administration (NASA), Goddard Space Flight
 Center (GSFC), Greenbelt, MD 20771, USA.*

^f*University of Maryland, College Park, MD 20742, USA*

Abstract

We measured atmospheric antiproton spectra in the energy range 0.2 to 3.4 GeV, at sea level and at balloon altitude in the atmospheric depth range 4.5 to 26 g/cm². The observed energy spectra, including our previous measurements at mountain altitude, were compared with estimated spectra calculated on various assumptions regarding the energy distribution of antiprotons that interacted with air nuclei.

Key words: atmospheric cosmic rays, cosmic-ray antiprotons, superconducting spectrometers

PACS: 13.85.Tp, 29.30.Aj, 95.85.Ry, 96.40.De,

* Corresponding author.

Email address: sanuki@icepp.s.u-tokyo.ac.jp (T. Sanuki).

¹ Present address: ICRR, The University of Tokyo, Kashiwa, Chiba 227-8582, Japan

² deceased.

³ Present address: JAEA, Tokai, Ibaraki 391-1195, Japan

1 Introduction

Antiprotons are produced in the atmosphere via interaction between cosmic rays and atmospheric nuclei. These atmospheric antiprotons are carrying important information about the physical processes of their production and propagation in the atmosphere. The production and propagation mechanisms should be similar to those of galactic antiprotons. Therefore the study of atmospheric antiprotons is important for understanding the energy spectrum of galactic antiprotons. In addition atmospheric antiprotons are a major background for the galactic antiprotons measured at balloon altitude. This background has to be estimated by model calculations. However model calculations of this background [1,2,3,4,5,6] have not yet been verified by direct observation.

We report here the atmospheric antiproton spectra measured with the BESS detector in a kinetic energy region of 0.2 – 3.4 GeV at sea level at the atmospheric depth 994 g/cm² in 1997 (BESS-1997), and at balloon altitude over the atmospheric depth range 4.5 – 26 g/cm² in 2001 (BESS-2001). The antiprotons observed at balloon altitude are assured not to be primary, but are produced inside the atmosphere, because the vertical geomagnetic cut-off energy was 3.4 GeV for protons/antiprotons throughout the balloon flight. The measured spectra, including our previous data observed at mountain altitude at the atmospheric depth 742 g/cm² in 1999 [7], will be compared with two model calculations. We will discuss how these calculations provide fits to the observed data.

2 The BESS spectrometer

The detector for the Balloon-borne Experiment with a Superconducting Spectrometer (BESS) was designed [8,9] and developed [10,11,12,13] as a high-resolution magnetic-rigidity spectrometer with a large acceptance to perform highly sensitive searches for rare cosmic-ray components, as well as precise measurements of various cosmic-ray species [14,15,16]. A uniform magnetic field of 1 Tesla is produced by a thin superconducting solenoid [17]. The magnetic-rigidity ($R \equiv Pc/Ze$) of an incoming charged particle is measured by a tracking system which consists of a jet-type drift chamber and two inner drift chambers inside the magnetic field. The deflection (R^{-1}) is calculated for each event by applying a circular fit using up to 28 hit points, each with a spatial resolution of 200 μm . Upper and lower scintillator hodoscopes [13] provide time-of-flight and two independent dE/dx measurements. Time resolution of each counter is 55 ps, resulting in a $1/\beta$ resolution of 1.4%, where β is defined as the particle velocity normalized by the speed of light. The first-level trigger

is provided by a coincidence between the top and the bottom scintillators with the threshold set at 1/3 of the pulse height for minimum ionizing particles. In the BESS-1997 ground experiment, all the first-level triggered events were recorded because the trigger rate was 30 Hz, which is low enough to record all the events. In the BESS-2001 balloon-flight experiment, the first-level trigger rate was too high to record all the events, and thus a second-level trigger was issued when a particle's rigidity was calculated to be negative by the onboard computer [11,18] to record negatively charged particles preferentially. In addition to this biased trigger mode, one out of every four first-level triggered events were recorded to provide an unbiased data sample in the balloon flight. The BESS instrument also incorporates a threshold-type Cherenkov counter [12], whose radiator was a silica-aerogel with a reflective index of 1.03 in BESS-1997 and 1.02 in BESS-2001. Antiprotons are distinguished from e^- and μ^- background by imposing that there be no light output from the Cherenkov counter. The rejection factor in this analysis was about 50,000 and 7,000 in BESS-1997 and BESS-2001, respectively.

3 Observations

The BESS-1997 observations at sea level were carried out at the High Energy Accelerator Research Organization (KEK), Tsukuba, Japan ($36^\circ 12' \text{ N}$, $140^\circ 6' \text{ E}$), where the geomagnetic cut-off rigidity was 11.2 GV, during the two periods of 6th – 11th May, and 7th – 13th December in 1997. The BESS-2001 balloon flight was carried out at Ft. Sumner, New Mexico, USA ($34^\circ 49' \text{ N}$, $104^\circ 22' \text{ W}$) on 24th September 2001. Throughout the flight, the vertical geomagnetic cut-off rigidity was about 4.2 GV, which corresponds to a kinetic energy of 3.4 GeV for protons/antiprotons. After the balloon reached a normal floating altitude of 37 km, where the atmospheric depth is 4.5 g/cm^2 , it began to lose altitude and continued descending for 13 hours before the termination of the flight at an atmospheric depth of around 30 g/cm^2 . The atmospheric depths throughout the observations are shown in Fig. 1. The mean atmospheric depth during sea level and balloon altitude observations was 994 g/cm^2 and 10.7 g/cm^2 , respectively.

4 Data analysis

Analysis was performed in the same way as in the previous BESS experiments [14,19]. We first selected events without interactions inside the BESS detector and with good-quality measurements of the rigidity and velocity. Particle identification was performed by requiring that dE/dx be consistent

with a singly charged particle, no signal was observed from the silica-aerogel Cherenkov counter, and particle mass was calculated to be consistent with the antiproton mass. In Fig. 2, events between the two curves were identified as antiprotons. The number of detected antiproton candidates in the energy range 0.2 - 3.4 GeV were 25 at sea-level in BESS-1997 and 156 at balloon altitude in BESS-2001.

In order to obtain the absolute flux of antiprotons at the top of the BESS instrument, we estimated the event selection efficiency, interaction loss probability and energy loss inside the instrument, and background contamination. The selection efficiency was obtained by using the recorded data, which consist mainly of protons since dE/dx and $1/\beta$ are the same as those of antiprotons. The interaction probability and energy loss inside the instrument, as well as its geometrical acceptance, were calculated by Monte Carlo (MC) simulation. The MC code was tuned and verified by comparing the simulation with an accelerator beam test of the BESS detector [20]. The systematic uncertainty of the event selection efficiency and antiproton interaction losses were evaluated to be 5% from this beam test. The background contamination due to inefficiency of the silica-aerogel Cherenkov counter was estimated by dividing N^- by the rejection factor of the Cherenkov counter, where N^- is the number of negatively charged particles after applying all selection cuts except for the Cherenkov veto to the entire set of events. The rejection factor was estimated using the recorded proton events during the balloon flight. In the energy range between 1.9 and 3.4 GeV, the background contamination was found to be 20% and 5% in BESS-1997 and BESS-2001, respectively. Between 1.0 and 1.9 GeV, the contamination was less than 1% for both observations. Below 1.0 GeV, it was negligibly small.

Fig. 3 shows the resultant antiproton flux observed at sea level in BESS-1997 and at balloon altitude in BESS-2001. These results are summarized in Tables 1 and 2. The detectable energy range was limited by the threshold of the silica-aerogel Cherenkov counter's ability to reject background in BESS-1997. As for the BESS-2001 experiment, the upper limit of the energy range was set not to exceed the geomagnetic cut-off energy. Results of the model calculations discussed below, as well as our previously published data obtained at mountain altitude [7], are also shown in Fig. 3.

5 Model calculations

Several calculations of the atmospheric antiproton flux have been published [1,2,3,4,5,6]. We made a phenomenological calculation of atmospheric antiproton flux under the observation conditions, following those model calculations. Referring to the transport equation given by Stephens [4], we solved the following equa-

tion:

$$\begin{aligned} \frac{\partial J_{\bar{p}}(E, x)}{\partial x} = & \sum_A Q_A(E_A, x, E) + \frac{\partial}{\partial E} \left[J_{\bar{p}}(E, x) \left\langle \frac{dE}{dx} \right\rangle \right] - \frac{J_{\bar{p}}(E, x)}{\Lambda(E)} \\ & + \int_E^\infty \Phi(E, E') \left[(1 - \alpha) \frac{J_{\bar{p}}(E', x)}{\lambda^{in}(E')} + \alpha \frac{J_{\bar{n}}(E', x)}{\lambda^{in}(E')} \right] dE' \end{aligned} \quad (1)$$

Here, $J_{\bar{p}}(E, x)$ is the differential antiproton flux at the atmospheric depth x g/cm². The first term on the right-hand side, $Q_A(E_A, x, E)$, represents the production rate of antiprotons with energy E by the incident particle A with energy E_A . Since the flux of incident particles depends on the atmospheric depth x , $Q_A(E_A, x, E)$ is a function of x . The second term represents the flux change due to the ionization energy loss. The average energy loss per g/cm² is indicated by $\langle dE/dx \rangle$. The third term represents loss of antiprotons due to interactions. $\Lambda(E)$ is the total inelastic interaction mean free path (mfp). It is described as $\Lambda(E) = [1/\lambda^{ann}(E) + 1/\lambda^{in}(E)]^{-1}$, where $\lambda^{ann}(E)$ and $\lambda^{in}(E)$ are mfp's for annihilating and non-annihilating processes of antiprotons passing through the atmosphere, respectively. The fourth integral term represents the tertiary antiproton production rate by non-annihilative inelastic interaction. $\Phi(E, E')$ signifies the probability that an antiproton with initial energy of E' possesses energy E after a collision. The charge exchange probability between antiprotons and antineutrons is described as α , which is taken to be 1/3. Therefore $\Phi(E, E')(1 - \alpha)J(E')_{\bar{p}}/\lambda^{in}(E') dE'$ represents the production rate of tertiary antiprotons with energy of E by the parent antiproton with an energy between E' and $E' + dE'$. In addition to the tertiary production from antiprotons, a contribution from antineutrons (\bar{n}) is also included in this integral term.

The primary cosmic-ray flux used in this calculation was based on the results from the BESS-98 [15] and AMS [21] experiments, the results of which are in good agreement. The proton, neutron, and helium fluxes at various atmospheric depths were obtained by using the transport equation, and a contribution from heavier nuclei such as CNO was included, following Papini et al. [22]. The antiproton production spectrum by the cosmic rays was taken from Stephens's formulation [4].

The mfp's, $\Lambda(E)$, $\lambda^{in}(E)$ and $\lambda^{ann}(E)$, are the same as those adopted by Stephens [4]. These are shown in Fig. 4. The details of the parameters are explained by Stephens [4] and by Tan and Ng [23].

Since there is no direct experimental data on antiproton energy distribution after collision with the air target, we examined several forms of $\Phi(E, E')$ in this study. One was very similar to those adopted by Bowen and Moats [1], Stephens [4] and Tan and Ng [23]. In this model, $\Phi(E, E')$ was assumed to be of

the form of $1/E'(0 \leq E \leq E')$, which means the probability that an antiproton with initial energy E' possesses energy E after a collision is uniform from $E = 0$ to $E = E'$. The average energy after a collision is half of the initial energy. We call this model a “box-approximation”, because the energy distribution of produced tertiary antiprotons has a box-shaped spectrum. Another model was proposed by Huang on a different assumption [5]. In his evaluation of total inelastic interaction, only annihilation channels were taken into account in the inelastic interactions. Non-annihilating inelastic processes were not included as a process of antiproton energy loss. This assumption corresponds to taking $\Phi(E, E') = \delta(E' - E)$. This is an extreme case in which a tertiary antiproton does not lose its energy in a collision with an atmospheric nucleus. We call this model a “ δ -approximation”. Other intermediate models between the above two models could be considered, such as $\Phi(E, E') = 1/(E' - E'')(E'' \leq E \leq E')$, where E'' is taken to be various between 0 and E' . The box- and δ -approximations correspond to taking E'' as 0 and E' , respectively.

In order to compare the observed flux with the calculated results, the following two effects were taken into account: the dependence of the geometrical acceptance and antiproton flux on the zenith angle, and the effective observation time at each atmospheric depth. The weighted averaged flux taking into account these points, $\langle J_{\bar{p}}(E) \rangle$, was defined as

$$\langle J_{\bar{p}}(E) \rangle \equiv \frac{\int_0^{+1} d(\cos \theta) \int_{x_1}^{x_2} dx J_{\bar{p}}(E, x^*(x, \theta)) \Delta T(x_1, x_2) \Delta S \Omega(E, \cos \theta)}{\int_0^{+1} d(\cos \theta) \int_{x_1}^{x_2} dx \Delta T(x_1, x_2) \Delta S \Omega(E, \cos \theta)}, \quad (2)$$

where $J_{\bar{p}}$ is a solution of Eq. (1) and x^* denotes the effective atmospheric depth, which depends on zenith angle of incoming parent particles. $\Delta T(x_1, x_2)$ is the live observation time between atmospheric depth x_1 and x_2 . $\Delta S \Omega(E, \cos \theta)$ is the geometrical acceptance corresponding to the energy and range of zenith angle, obtained by the MC simulation. In the calculation for balloon altitude, the zenith angle dependence of antiprotons was assumed to be $x^*(x, \theta) = x/\cos \theta$, because the number of antiprotons produced should be proportional to the path length of the primary parent particle. On the other hand, since the tertiary antiprotons dominate in those observed at large atmospheric depth, they might have collided with nuclei several times and changed their directions. In this case, their flux is very sensitive to the mfp inside the atmosphere, and their real path length cannot be inferred from the observed zenith angle. We simply assumed $x^*(x, \theta) = x$ in this study. This assumption does not significantly change the antiproton spectral shape, but may change its absolute flux at a large atmospheric depth.

6 Results and discussions

The resultant energy spectra of antiprotons observed at sea level (BESS-1997) and at balloon altitude (BESS-2001) are shown in Fig. 3. These results are compared with our previous data observed at Mt. Norikura, Japan [7], where the mean atmospheric depth was 742 g/cm^2 , together with the results of the corresponding model calculations. Since the primary galactic antiproton flux was taken into account in the calculation, a sharp edge is seen at the cut-off energy of around 3.5 GeV in the calculated flux at $4.5 - 26 \text{ g/cm}^2$ at Ft. Sumner. Here, we adopted the galactic antiproton spectrum calculated by Mitsui [3] with the solar activity characterized by $\Phi = 1000 \text{ MV}$. The antiprotons observed at balloon altitudes are assured to be purely atmospheric because the highest energy of the measurement is below the geomagnetic cut-off energy.

The antiproton energy spectrum at small atmospheric depth is mainly determined by the production rate of secondary antiprotons, $\sum_A Q_A(E_A, x, E)$ in Eq. (1), and the tertiary antiprotons are not dominant. The model calculations based both on box- and δ -approximations reproduced the energy spectrum observed at balloon altitude, where secondary antiprotons are dominant over tertiary ones. It suggests the production energy spectrum of secondary antiprotons was properly treated in our calculation.

At large atmospheric depth, tertiary antiprotons dominate over secondary ones. The calculation results with the box-approximation show good agreement with observed data at mountain altitude and sea level above 1 GeV. The box-approximation was developed by comparing calculated and observed proton spectra at sea level and mountain altitude above 1 GeV in previous works by Bowen and Moats [1], and Stephens [4]. The observed spectra were reproduced well by the box-approximation above 1 GeV, but below 1 GeV the δ -approximation matches the data more closely. Calculation results with the box-approximation show that the energy spectrum is almost flat in a lower energy region both at sea level and mountain altitude. However, the energy spectra obtained in the δ -approximation decrease below 1 GeV irrespective of observation altitude. A model calculation based on a combination of the box- and δ -approximations may therefore reproduce the observed spectra better over a wider energy range than the simple box- or δ -approximation. Some accelerator experimental results indicate that the shape of the probability function $\Phi(E, E')$ changes depending on the initial energy of a projectile particle [3]. Measurement of the atmospheric antiproton spectrum with better statistical accuracy over a wider energy range would help to estimate a proper shape of $\Phi(E, E')$.

7 Conclusion

We measured the atmospheric antiproton spectrum at $4.5 - 26 \text{ g/cm}^2$ and at sea level in the kinetic energy range $0.2 - 3.4 \text{ GeV}$ for the first time.

We also referred to our previous observed data at Mt. Norikura in 1999 [7] to study the propagation of antiprotons in the atmosphere. The energy spectra of antiprotons were calculated for the balloon altitude, mountain altitude and sea level. The model calculations based both on box- and δ -approximations reproduced the energy spectrum observed at balloon altitude, where secondary antiprotons are dominant over tertiary ones. This suggests the production energy spectrum of secondary antiprotons was properly treated in our calculation. The spectral shapes of our three measurements below 1 GeV were reproduced by the δ -approximation, while the calculated flux amplitude at larger depths and higher energies was not well-matched to the data. The opposite is true for the box-approximation, which matched the flux data above 1 GeV , but was not well-matched to the data at larger depths and lower energies. A model calculation based on a combination of the box- and δ -approximations may reproduce the observed spectra better over a wider energy range than the simple box- or δ -approximation.

Our measurement of antiproton spectra in the atmosphere suggests that the shape of the probability function $\Phi(E, E')$ depends on the initial energy of the projectile particle. Measurement of the atmospheric antiproton spectrum with better statistical accuracy over a wider energy range is highly desirable to improve accuracy of the model calculations.

Acknowledgements

We would like to thank NASA/GSFC/WFF BPO and NSBF for their collaboration and making possible the balloon expedition. We also thank KEK, ISAS, ICEPP/The University of Tokyo, and RESCEU/The University of Tokyo for continuous support. This experiment was supported in Japan by KAKENHI (12047206 and 12047227) from MEXT.

References

- [1] T. Bowen and A. Moats Phys. Rev. D 33 (1986) 651.
- [2] Ch. Pfeifer et al. Phys. Rev. C 54 (1996) 882.
- [3] T. Mitsui Ph. D. Thesis. The university of Tokyo (1996).
- [4] S. A. Stephens Astropart. Phys. 6 (1997) 229.
- [5] C. Y. Huang et al. Ph. D. Thesis. University Joseph Fourier (2003).
- [6] C. Y. Huang et al. Phys. Rev. D 68 (2003) 053008.
- [7] T. Sanuki et al. Phys. Lett. B 577 (2003) 10.
- [8] S. Orito et al. ASTROMAG Workshop. High Energy Accelerator Research Organization (KEK), Japan (1987) 111.
- [9] A. Yamamoto et al. IEEE Trans. Magn. 24 (1988) 1421.
- [10] A. Yamamoto et al. Adv. Space Res. 14 (1994) 75.
- [11] Y. Ajima et al. Instrum. Methods Phys. Res., Sect. A 443 (2000) 71.
- [12] Y. Asaoka et al. Instrum. Methods Phys. Res., Sect. A 416 (1998) 236.
- [13] Y. Shikaze et al. Instrum. Methods Phys. Res., Sect. A 455 (2000) 596.
- [14] Y. Asaoka et al. Phys. Rev. Lett. 88 (2002) 051101.
- [15] T. Sanuki et al. Astrophys. J. 545 (2000) 1135.
- [16] K. Abe et al. Phys. Lett. B 564 (2003) 8.
- [17] Y. Makida et al. IEEE Trans. Appl. Supercond. 5 (1995) 638.
- [18] T. Maeno et al. Astropart. Phys. 16 (2001) 121.
- [19] S. Orito et al. Phys. Rev. Lett. 84 (2000) 1080.
- [20] Y. Asaoka et al. Nucl. Instr. and Methods A 88 (2002) 170.
- [21] J. Alearaz ant others Phys. Lett. B 472 (2000) 215.
- [22] P. Papini, C. Grimani and S. A. Stephens Nuovo Cimento C 19 (1996) 367.
- [23] L. C. Tan and L. K. Ng J. Phys. G 9 (1983) 227.

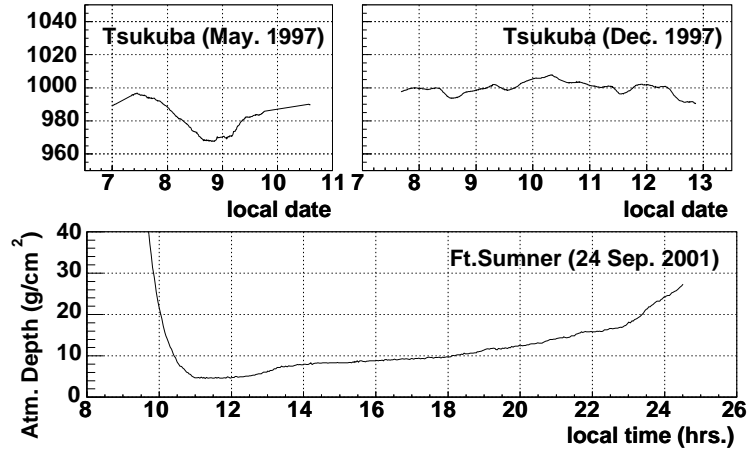


Fig. 1. Atmospheric depth during the BESS-1997 ground observations and the BESS-2001 balloon flight.

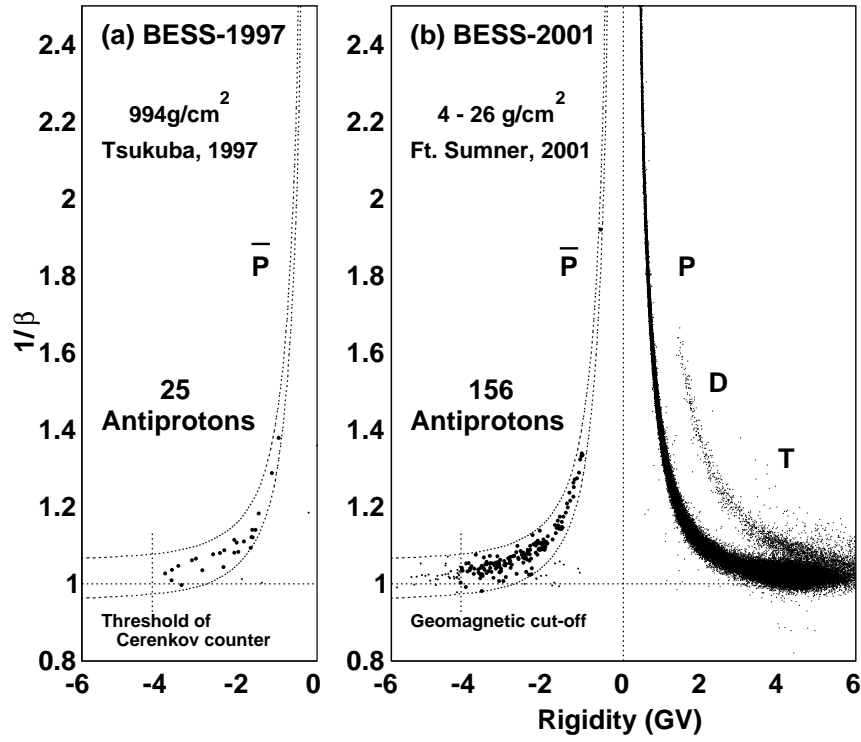


Fig. 2. The identification plots of antiproton events for (a) the BESS-1997 observations at sea level, and (b) the BESS-2001 balloon flight. The dotted curves define the antiproton mass bands.

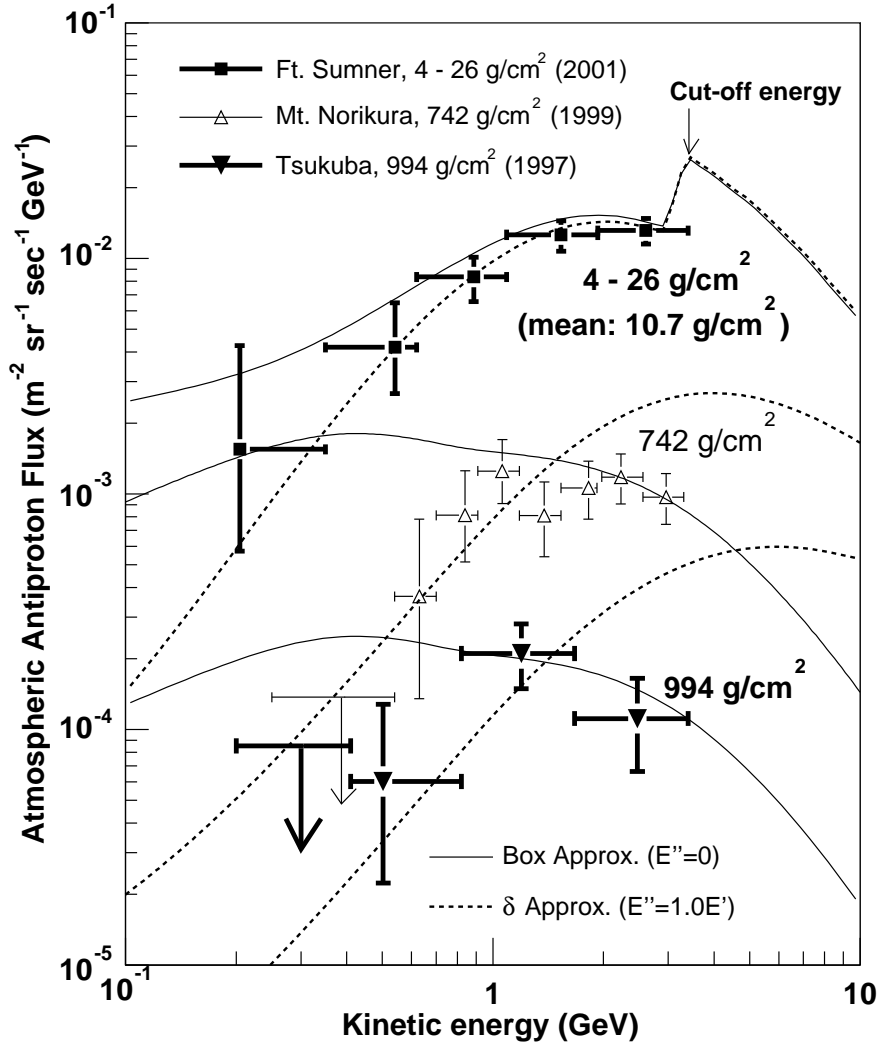


Fig. 3. The observed antiproton flux at atmospheric depth of 4.5 - 26 g/cm² at Ft. Sumner in 2001 and at 994 g/cm² at Tsukuba in 1997. The flux at 742 g/cm² at Mt. Norikura [7] is also shown. The results are compared with calculations assuming box-approximation (solid lines) and δ -approximation (dashed lines).

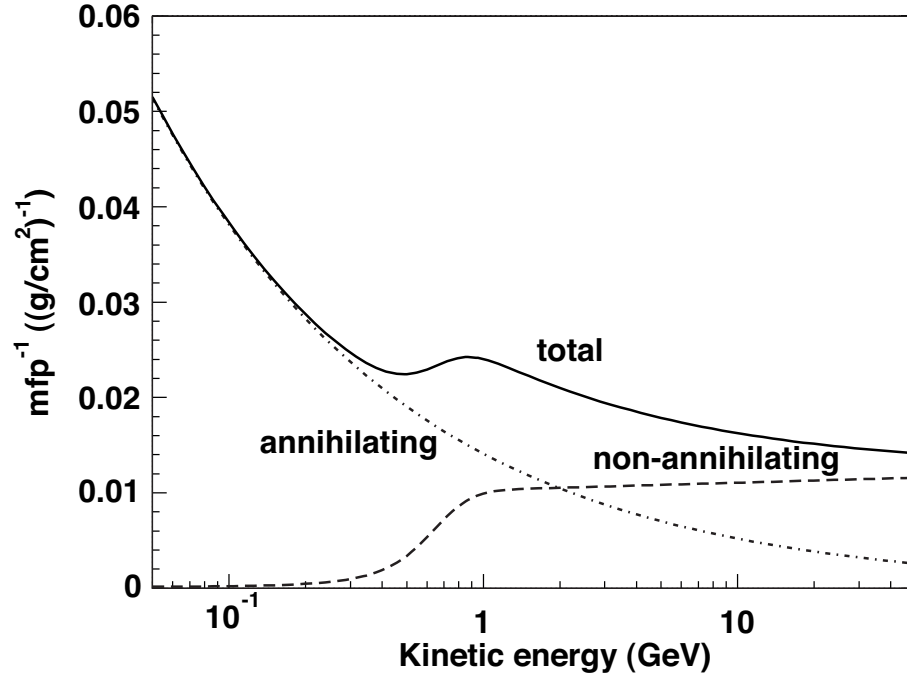


Fig. 4. Mean free paths assumed in the calculations.

Table 1

Observed antiproton flux at sea level, 994 g/cm² at Tsukuba in 1997.

Kinetic energy (GeV)		Numbers		Antiproton flux
range	mean	antiproton	background	(m ⁻² sr ⁻¹ s ⁻¹ GeV ⁻¹)
0.20–0.41	-	0	0.0	8.51 × 10 ⁻⁵ upper limit
0.41–0.82	0.50	2	0.0	6.02 ^{+6.77+0.10} _{-3.79-0.11} × 10 ⁻⁵
0.82–1.67	1.19	13	0.1	2.10 ^{+0.70+0.07} _{-0.60-0.07} × 10 ⁻⁴
1.67–3.40	2.47	10	1.9	1.11 ^{+0.52+0.12} _{-0.44-0.08} × 10 ⁻⁴

Table 2

Observed antiproton flux at the atmospheric depth of 4.5 - 26 g/cm² at Ft. Sumner in 2001.

Kinetic energy (GeV)		Numbers		Antiproton flux
range	mean	antiproton	background	(m ⁻² sr ⁻¹ s ⁻¹ GeV ⁻¹)
0.20–0.35	0.20	1	0.0	1.55 ^{+2.71+0.06} _{-0.97-0.06} × 10 ⁻³
0.35–0.62	0.54	6	0.0	4.19 ^{+2.29+0.04} _{-1.52-0.04} × 10 ⁻³
0.62–1.09	0.89	22	0.0	8.34 ^{+1.78+0.24} _{-1.78-0.24} × 10 ⁻³
1.09–1.93	1.53	50	0.4	1.26 ^{+0.18+0.05} _{-0.18-0.05} × 10 ⁻²
1.93–3.40	2.61	77	4.0	1.31 ^{+0.15+0.06} _{-0.15-0.06} × 10 ⁻²